Received January 2003
Revised August 2003
Accepted September 2003

The effect of tube wall heat conduction on the natural convection in a long cylindrical envelope with an adiabatic lateral surface

He Ya-Ling, Ding Wen-Jing and Tao Wen-Quan
School of Energy and Power Engineering, Xi'an Jiaotong University, Xi'an, People's Republic of China

Keywords *Convection, Modelling, Numerical analysis, Heat transfer*

Abstract *The effect of the tube wall heat conduction on the natural convection in a tilted long cylindrical envelope with constant, but different temperature of the two ends and an adiabatic outer surface was numerically investigated. The envelope is supposed to be a simplified model for the pulse tube in a pulse tube refrigerator when the pulse tube is positioned at different orientations. It is found that the cylindrical envelope lateral wall heat conduction can enhance the heat transfer from the hot end to the cold end, not only because of the increase in pure heat conduction in the wall, but more importantly, also the intensification of the natural convection within the enclosure. This enhancement is resulted from the big temperature difference between the tube wall and the adjacent fluid near the hot and cold ends. Adoption of low thermal conductivity tube can effectively reduce such additional heat transfers from hot to cold end, thus reducing the loss of cooling capacity for the pulse tube refrigerator.*

Nomenclature

a	= fluid thermal diffusivity	S	= source term
c_p	= specific heat at constant pressure	SMAX	= maximum absolute value of mass flow rate residual of control volume
d	= diameter		
E_b	= emmisive power of black body		
g	= gravitational acceleration	SSUM	= summation of mass flow rate residual of all control volume in the computational domain
L	= length of the pulse tube		
p	= pressure		
Pr	= Prandtl number	T	= temperature
Q	= heat transfer rate	u, v, w	= velocity component in circumferential, radial and axial coordinate
R	= radius		
Ra_D	$= g\beta(T_h - T_c)d^3/(av)$		
Ra_L	$= g\beta(T_h - T_c)L^3/(av)$	X	= angle factor
R_t	= radiative thermal resistance	z	= axial coordinate
Greek symbols		δ	= tube wall thickness
β	= volume expansion coefficient	ε	= surface emissivity
Γ	= nominal diffusion coefficient	η	= fluid dynamic viscosity

International Journal of Numerical Methods for Heat & Fluid Flow
Vol. 14 No. 8, 2004
pp. 918-952

0961-5539
DOI 10.1108/09615530410539982

The work reported here was supported by the National Key Project of R&D in China (G2000026303) and the National Natural Science Foundation of China (Grant No. 50276046). The authors are also grateful to the reviewers for their valuable comments.

λ_w	= wall thermal conductivity	*Subscripts*	
ν	= fluid kinetic viscosity	a	= adiabatic
θ	= inclination angle	c	= cold
ρ	= fluid density	cond	= conduction
ϕ	= general variable	h	= hot
φ	= circumferential angle	m	= mean

1. Introduction

Natural convection in enclosures is a classical problem in both experimental and numerical heat transfer, and many studies have been performed (Barakos and Mitsoulis, 1994; Charrie-Mojtabi *et al.*, 1979; Date, 1986; De Vahl Davis, 1983; Hortman and Peric, 1994; Keyhani *et al.*, 1983; Kuehn and Goldstein, 1976, 1980; Ozoe *et al.*, 1985; Saitoh and Hirose, 1989; Wei and Tao, 1996a, b). However, most of the earlier numerical investigations were based on the following conditions.

(1) Boussinesq assumption was adopted, which is valid for a limited value of temperature difference between the hot and cold surfaces (Gary and Giorgin, 1976). For example, for air at room temperature, within a deviation of 10 per cent, the maximum temperature difference for adoption of this assumption is below 40 K (Lankhorst, 1991).

(2) As far as the geometric shape is concerned, most studies were conducted for rectangular enclosures (Barakos and Mitsoulis, 1994; De Vahl Davis, 1983; Hortman and Peric, 1994; Ozoe *et al.*, 1985; Saitoh and Hirose, 1989) or annulus (Charrie-Mojtabi *et al.*, 1979; Date, 1986; Keyhani *et al.*, 1983; Kuehn and Goldstein, 1976; Wei and Tao, 1996a, b).

Very few investigations were conducted for a long cylindrical envelope with two ends being maintained at constant, but different temperatures, in spite of its common existence in various engineering applications. A search of literature only revealed several papers (Bejan and Tien, 1978; Edwards and Catton, 1969; Kimura and Bejan, 1980), among which those of Bejan and Tien (1978) and Edwards and Catton (1969) are theoretical works based on Boussinesq assumption, and that of Kimura and Bejan (1980) is an experimental study for water with a maximum temperature difference about 70°C. One typical application example is the pulse tube of pulse tube refrigerator. The schematic diagram of pulse tube refrigerator is shown in Figure 1. Pulse tube refrigerator is an attractive cryocooler of small capacity widely used in aerospace engineering and for military purposes because of its inherent advantages such as no moving parts in the cold stage, low manufacturing cost, reduced mechanical vibration, etc. As shown in Figure 1, the pulse tube itself is a long tube with an inner diameter ranging from several millimeters to tens millimeters, and its two ends can be regarded as two isothermal surfaces. The pulse tube may be connected with the pressure wave generator by a long flexible tube with a length of several meters, thereby reducing the interference of noise from the compressor and rotary valve to a negligible level. The flexible connectivity between compressor and cold end also allows one to change the orientation of the pulse tube, which is an attractive feature for application. The fluid flow in the pulse tube system is oscillating, with frequency ranging from 2 Hz to tens of Hz. The different orientation of the pulse tube leads to different relative positions of the hot and cold ends, which may cause natural convection in the enclosure when

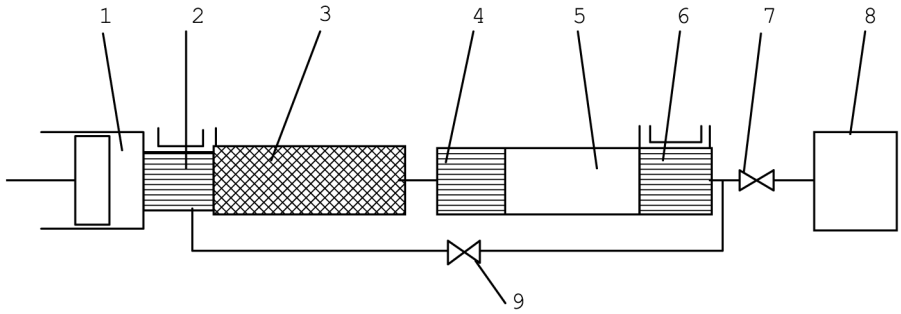

Figure 1.
Schematic diagram of pulse tube refrigerator

1. Pressure wave generator 2. Water cooler 3. Regenerator 4. Cold end heat exchanger
5. Pulse tube 6. Hot end heat exchanger 7. Orifice valve 8. Reservoir 9. Double inlet valve

the frequency is low. As a first approximation, the forced convection of the pulsating streaming and the natural convection due to temperature difference may be decoupled (Thummes *et al.*, 1997), and the respective flow can be investigated in detail to reveal its inherent characteristics. For a pulse tube refrigerator with low frequency, the existence of such a natural convection may have appreciable effect on the cooling capacity loss, as will be seen from the predicted results. From heat transfer point of view, this is a natural convection in a long cylindrical envelope. The temperature difference between the hot and cold ends may be as large as 220 K or more, the conventional Boussinesq assumption by no means applicable, and a full consideration of the variable thermal properties must be taken in the analysis of the natural convection. Within the authors' knowledge, such a problem has not been reported in the published papers.

The geometry of the present study is now presented. A tilted cylindrical envelope is shown in Figure 2, where the origin of the Z coordinate is fixed at the hot end and θ is the angle between the axis of the pulse tube and the gravity. When $\theta = 0°$, the hot end

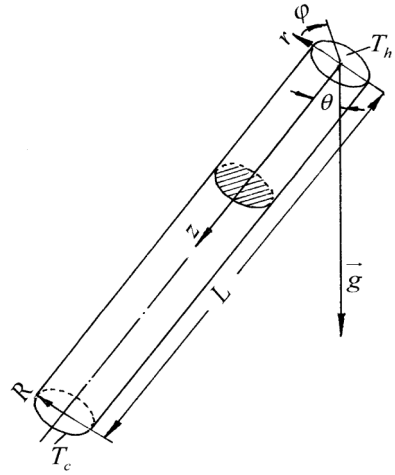

Figure 2.
Coordinates and geometry of the cylindrical envelope

is up and the cold end is down; while for $\theta = 180°$, the situation is the opposite. Thummes *et al.* (1997) reported their experiments in this regard, and found a profound effect of the natural convection in the pulse tube on the cooling capacity of a PTR (Thummes *et al.*, 1997). They also adopted some available heat transfer correlations for the natural convection in cylindrical enclosures at different orientations and estimated the heat transfer rate by these correlations. They obtained the heat transfer rate of the natural convection in the pulse tube from their experimental net cooling power and from the prediction of the correlations. In the θ range from 0 to 70°, and at $\theta = 180°$, they obtained qualitative agreement, while in the range of $\theta = 70$-180° the correlations they adopted only roughly describes the observed variation of heat transfer rate. According to author's, such result may be expected since the correlations they adopted are all based on the small temperature difference cases, which cannot take the effect of the severe variation in thermal physical properties into account. According to Kays and Crawford (1980), the Boussinesq assumption is a two-part approximation:

(1) it neglects all variable properties effects in the governing equations, except for the density in the momentum equations and

(2) it approximates the density difference term with simplified equations of state:

$$\rho_r - \rho = \rho\beta(t - t_r) \tag{1}$$

where β is the volumetric coefficient of thermal expansion (for ideal gas $\beta = 1/T_r$), and t_r is a reference temperature.

In our computation, the hot end is set at 300 K, and the cold end at 80 K. The temperature difference is as large as 220 K. The variation of thermal conductivity and dynamic viscosity of helium is more than a factor of 2 (Table I). Thus, the above-mentioned Boussinesq assumption is not acceptable, and the variations of the thermal properties (including density) with temperature in all terms of the governing equations should be considered. This was implemented by introducing the curve-fitting equations for λ, η, c_p and Pr in the code based on the data provided by Barron (1999), and before every iteration the thermophysical properties were calculated from the available temperature field. The gas density was determined by using the state equation of perfect gas. To demonstrate the necessity of such a practice, comparative computational results will be presented later.

As indicated above, the only experimental work published so far is that of Kimura and Bejan (1980). They performed an experimental study for the natural convection of water in a horizontal tube with the two ends at different, but constant temperatures. The Rayleigh number based on the tube diameter was ranged from 10^8 to 10^9, with the end temperature difference around 70°C. They found that at each cross section normal to the axial direction, the temperature depth variation along the vertical diameter is almost linear. In addition, in the cross section through the *z-r* plane, the measured

Property	300 K	80 K
Thermal conductivity (W/m K)	1.505×10^{-1}	6.404×10^{-1}
Dynamic viscosity (kg/m s)	1.987×10^{-5}	8.200×10^{-6}
Density kg/m^3	2.888	1.083×10^{1}
Prandtl number	0.6874	0.6658

Table I. Thermophysical properties of helium

velocity distributions show that the flow consists of two jets, one flowing towards the cold end along the top surface and the other flowing in the opposite direction along the bottom. Some qualitative comparisons of our numerical predictions and the test results of Kimura and Bejan (1980) will be made later in this paper.

He and coworkers (He, 2002; He *et al.*, 2004a, b) performed three-dimensional numerical simulation for the natural convection in a simplified pulse tube model. Rather than adopting the Boussinesq assumption, they considered the variation of the thermal properties with temperature. But they neglected the effect of the heat conduction in the lateral wall. The predicted curve pattern of the heat loss with the inclined angle provided in He (2002) and He *et al.* (2004a, b) is quite similar to the experimental results shown in Thummes *et al.* (1997), but quantitatively, the numerical value is lower than the experimental one by about 20-25 per cent. A major reason was attributed to the neglect of the lateral wall heat conduction (He, 2002).

The effect of wall heat conduction on the natural convection in a rectangular enclosure has been the object of previous work (Costa, 2002; Du and Bilgen, 1992; Ho and Lin, 1989, 1990; Ho *et al.*, 1989; Kim and Viakanta, 1985). Generally speaking, these studies reveal that heat transfer and fluid flow in the enclosure is strongly influenced by the coupling between the solid wall conduction and fluid convection. However, most earlier studies focused on the rectangular enclosure with diffusive vertical walls and adiabatic top/bottom surfaces or vertical cylindrical enclosure with diffusive vertical wall and adiabatic top/bottom surfaces. These situations are quite different from the present case, hence specific conclusions resulting from earlier investigations cannot be applied to the present case. In this paper, the effect of the lateral wall heat conduction on the natural convection in a tiled long cylindrical envelope with constant, but different temperatures of the two ends is numerically investigated. In the calculation, the Boussineq assumption is not adopted and the variations of the thermal properties with temperature are fully considered. The length of the tube is 250 mm. The inner diameter is 27.8 mm ($L/D = 9.0$) and the outer diameter is 29.8 mm (tube wall thickness equals 1 mm). The average pressure in the tube is 18 bar (He, 2002). Computations were conducted for every 10° increment starting from $\theta = 0°$. The working fluid is helium. These conditions are taken from He *et al.* (2004a, b) where the heat conduction in the lateral wall was totally neglected and the lateral wall was simply simulated by an adiabatic boundary condition.

In the following presentation, the three-dimensional governing equations of the physical problem will be presented first, followed by a brief description of the numerical methods. Then details of numerical results, including the velocity and temperature distributions will be provided. Analysis will be focused on why the tube wall heat conduction can significantly enhance the natural convection in the enclosure when the hot end is down. Finally, some conclusions will be drawn.

2. Governing equations

The problem considered can be outlined as follows. A tube with finite thickness contains helium within it. The two ends of the tube are kept at 300 and 80 K, respectively. The outside surface of the tube is adiabatic, and the tube can be positioned at any orientation. The heat transfer from the hot end to the cold end because of the natural convection and the tube lateral wall heat conduction is to be predicted. This problem is a conjugated one and the heat conduction in the lateral wall

should be predicted simultaneously with the fluid flow and heat transfer of the fluid within the tube.

The three-dimensional governing equations for fluid flow and heat transfer in a cylindrical envelope with variable thermal properties take the following form:

$$\frac{\partial}{\partial z}(\rho u\phi)+\frac{1}{r}\frac{\partial}{\partial r}(r\rho v\phi)+\frac{1}{r}\frac{\partial}{\partial \varphi}(\rho w\phi)=\frac{\partial}{\partial z}\left(\Gamma\frac{\partial \phi}{\partial z}\right)+\frac{1}{r}\frac{\partial}{\partial r}\left(\Gamma r\frac{\partial \phi}{\partial r}\right)+\frac{1}{r}\frac{\partial}{\partial \varphi}\left(\frac{\Gamma}{r}\frac{\partial \phi}{\partial \varphi}\right)+S \tag{2}$$

where ϕ is the general variable, representing u, v, w and T, Γ is the general diffusion coefficient, and S is the general source term. For a case with variable thermophysical properties, the general source term takes the following form for different variables:

$$u: S=-\frac{\partial p}{\partial z}+\frac{\partial}{\partial z}\left(\eta\frac{\partial u}{\partial z}\right)+\frac{1}{r}\frac{\partial}{\partial r}\left(r\eta\frac{\partial v}{\partial z}\right)+\frac{1}{r}\frac{\partial}{\partial \varphi}\left(\eta\frac{\partial w}{\partial z}\right)+\rho g\cos\theta \tag{3a}$$

$$v: S=-\frac{\partial p}{\partial r}+\frac{\partial}{\partial z}\left(\eta\frac{\partial u}{\partial r}\right)+\frac{1}{r}\frac{\partial}{\partial r}\left(r\eta\frac{\partial v}{\partial r}\right)+\frac{1}{r}\frac{\partial}{\partial \varphi}\left[\eta\frac{r\partial(w/r)}{\partial r}\right]-\frac{2\eta}{r}\left(\frac{1}{r}\frac{\partial w}{\partial \varphi}+\frac{v}{r}\right)+\frac{\rho w^2}{r}-\rho g\sin\theta\cos\varphi \tag{3b}$$

$$w: S=-\frac{1}{r}\frac{\partial p}{\partial \varphi}+\frac{\partial}{\partial z}\left(\eta\frac{\partial u}{r\partial \varphi}\right)+\frac{1}{r}\frac{\partial}{\partial r}\left[r\eta\left(\frac{1}{r}\frac{\partial v}{\partial \varphi}-\frac{w}{r}\right)\right]+\frac{1}{r}\frac{\partial}{\partial \varphi}\left[\eta\left(\frac{1}{r}\frac{\partial w}{\partial \varphi}+\frac{2v}{r}\right)\right]+\frac{\eta}{r}\left[r\frac{\partial(w/r)}{\partial \varphi}+\frac{1}{r}\frac{\partial v}{\partial \varphi}\right]-\frac{\rho vw}{r}+\rho g\sin\theta\sin\varphi \tag{3c}$$

It can be seen from equation (3) that apart from the pressure gradient term and gravitational term, quite a lot of terms of second derivatives of velocities exist, making the discretization and computational procedure very complicated. We adopt an assumption here to simplify the computation: the thermophysical properties in the velocity source term may be moved to the outside of the derivatives but still treated as a variable Then using the mass conservation law expressed by

$$\frac{\partial u}{\partial z}+\frac{1}{r}\frac{\partial}{\partial r}(rv)+\frac{1}{r}\frac{\partial w}{\partial \varphi}=0 \tag{4}$$

the source terms for the three components of velocity may be simplified as follows:

(1) In the fluid part of the pulse tube

$$u: S=-\frac{\partial p}{\partial z}+\rho g\cos\theta \tag{5a}$$

$$v : S = -\frac{\partial p}{\partial r} + \frac{\rho w^2}{r} - \frac{2\eta}{r^2}\frac{\partial u}{\partial \varphi} - \frac{\eta v}{r^2} - \rho g \sin\theta\cos\varphi \tag{5b}$$

$$w : S = -\frac{1}{r}\frac{\partial p}{\partial \varphi} - \frac{\rho w v}{r} + \frac{2\eta}{r^2}\frac{\partial v}{\partial \varphi} - \frac{\eta w}{r^2} + \rho g \sin\theta\sin\varphi \tag{5c}$$

It should be noted that the above mathematical formulations are also valid for the heat conduction in the solid wall by setting appropriate value of thermophysical properties and the source terms.

(2) In the solid part of the pulse tube

$$w : S = 0.0 \tag{6a}$$

$$v : S = 0.0 \tag{6b}$$

$$u : S = 0.0 \tag{6c}$$

The boundary conditions are depicted as follows:

For u, v, w: at all solid walls, $u = v = w = 0$; at the longitudinal cross section ($\varphi = 0$ and $\varphi = \pi$) symmetry condition is used, i.e.

$$w = 0, \quad \frac{\partial v}{\partial \varphi} = \frac{\partial u}{\partial \varphi} = 0$$

For T: at hot end ($z = 0$), $T = T_h$; at cold end ($z = L$), $T = T_c$; at the outer surface of the lateral wall ($r = R$), $\partial T/\partial r = 0$; at the longitudinal cross section ($\varphi = 0$ and $\varphi = \pi$) symmetry condition is used, $\partial T/\partial \varphi = 0$.

Some more words are added here about the symmetry boundary condition adopted in this study. It is well-known that for natural convection in enclosure under certain value of Ra number non-symmetrical fluid flow or even unsteady flow may be formed for steady and geometrically symmetrical condition (Powe *et al.*, 1969). In that case, transient and three-dimensional computations for the full envelope should be conducted. For the case studied, however, the value of Ra number is not high, and our predicted results from the present model agree well with some available experimental results (to be shown later). Thus, it is believed that the present model is an appropriate approximation for the problem studied.

3. Numerical methods

The fluid-solid conjugate heat transfer is solved by full-field computation method. Solid in computational domain is regarded as fluid of infinite viscosity. The same governing equations are applied for both fluid and solid. When the solid field was calculated the Γ of velocity is infinite (implemented by taking a very large number) (Patankar, 1980) and the Γ of temperature is defined as k/C_p, where k is the thermal conductivity of the solid and C_p is the specific heat at constant pressure of the fluid close to the lateral wall. In this program, C_p of the fluid was obtained from the equation $k/C_p = \eta/\mathrm{Pr}$, in which every parameter of the fluid uses local value. When the fluid field was calculated the Γ of velocity is η and the Γ of temperature is η/Pr. In the computations, two kinds of materials are considered: stainless steel and nylon.

Their thermal conductivity are taken as 10 and 0.25 W/m K, respectively. In order to further reveal the effect of the wall heat conduction, computations are also conducted for four more cases with wall thermal conductivity of 30, 60, 100, and 200 W/m K, respectively.

The governing equations are discretized by the finite volume method (Patankar, 1980; Tao, 2001). The diffusion and convection terms are discretized by the power-law scheme. The segregated solution algorithm, SIMPLEC, is adopted, where the momentum equations are solved one by one, the pressure field is updated from the mass conservation equation, and the pressure correction is used to revise both velocity components and pressure. The energy equation is coupled with the momentum equation via the source term, hence solved simultaneously with the momentum equations. The resulting algebraic equations are solved by successive line underrelaxation method. To guarantee the convergence of iteration, the relaxation factors for velocity components and temperature were all taken as 0.01. The temperature gradient at the hot and cold walls are determined by three-point second-order accurate discretized equation. The two-point formally first-order discretization formulation is also used. Comparison found that the numerical difference between these two discretized expressions is very small, always not being greater than 1 per cent.

The grid is distributed uniformly in the circumferential direction. In the radius direction, the grids are distributed uniformly in the pulse tube's solid part and in the fluid part individually, while in the axial direction, non-uniform distribution is adopted with more grids clustering near the two end walls. The grid number in three directions is $22(r) \times 20(\varphi) \times 80(z)$ (Figure 3). This grid system was based on the grid system adopted in He (2002) where a careful grid independent examination based on the total heat transfer rate between the hot and cold end was conducted for the case neglecting the tube wall heat conduction, and found that a grid system of $20(r) \times 20(\varphi) \times 80(z)$ (totally 32,000 grid points) can obtain grid-independent results (Figure 3(a)). In this study, two control volumes were added in the solid wall region. Based on Figure 3(a) a similar grid-independence examination is also conducted in the present work with two more control volumes being added in the lateral wall. Nine grid systems are examined, namely: $13 \times 15 \times 48$ (9360 in total), $15 \times 17 \times 60$ (15,300 in total), $18 \times 20 \times 64$ (23,040), $19 \times 21 \times 74$ (29,526), $20 \times 22 \times 80$ (35,200), $20 \times 22 \times 90$ (39,600), $22 \times 24 \times 90$ (47,520), $22 \times 24 \times 100$ (52,800) and $22 \times 24 \times 110$ (58,080). The variation of the average heat transfer rate with grid point is shown in Figure 3(b). As can be seen there, the numerical solution from the grid system with $20 \times 22 \times 80$ grid points can be considered as a grid-independent one. Thus, all the computations are conducted by using this grid system.

As indicated in He (2002) and He *et al.* (2004a, b), the problem at hand is a highly non-linear one and the thermophysical properties varies significantly along the axial direction. This makes the convergence of the iterative procedure very difficult. Numerical practices show that with zero velocity and linear temperature distributions as the initial fields, the cross-sectional axial flow rate, symbolized by GM, increases with the iteration first, reaches its maximum, and then approaches some steady value. The variation patterns of GM with iteration number (ITER) are presented for different orientations in Figures 4 and 5 (the tube wall thermal conductivity is 10 W/m K, where GM is defined as follows:

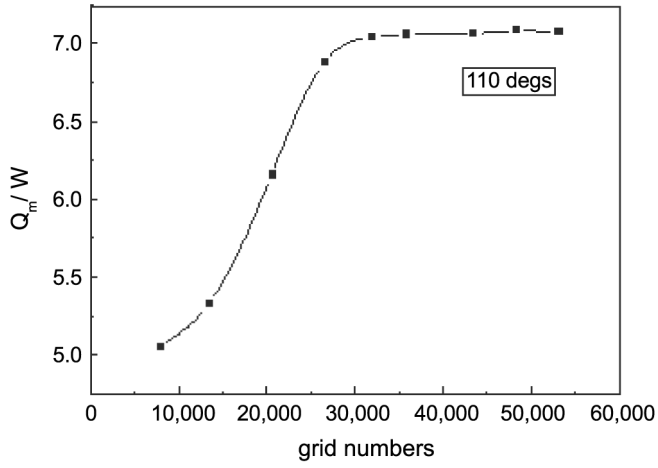

(a) Reference [21,22]

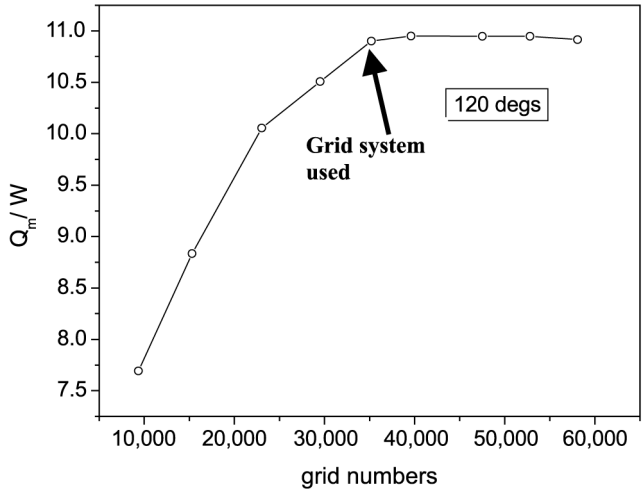

(b) Present study

Figure 3.
Grid-independence examination for the case of neglecting tube wall heat conduction

$$\mathrm{GM} = \frac{1}{N}\sum_{k=1}^{N}\int_{\Omega_k} \rho(i,j,k)abs(w(i,j,k))r\,\mathrm{d}r\,\mathrm{d}\varphi \tag{7}$$

where N is the number of section in axial direction (77 in total). Obviously, GM can be regarded as the section-average axial flow rate.

As seen in the figures, for the case of cold end down, the value of GM approaches constant after about 10,000 iterations, while for the case of hot end down, 30,000-40,000 iterations are needed. After that period GM keeps approximately constant.

According to such special feature of iteration process, we select the following criteria to judge the convergence of the iterative process.

(1) The cross-sectional average axial flow rate GM has been beyond the summit of GM-ITER curve and approaches almost constant within 200 consecutive iterations.

(2) The relative change in mean heat transfer rate between two consecutive iterations is less than 1×10^{-4};

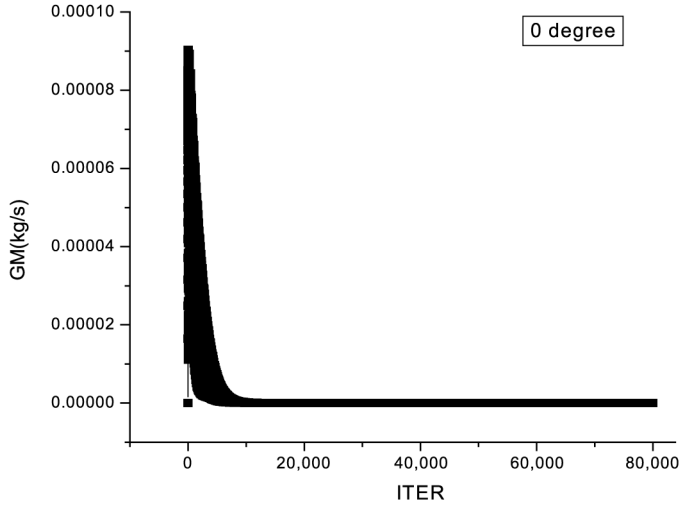

(a) $\theta = 0°$

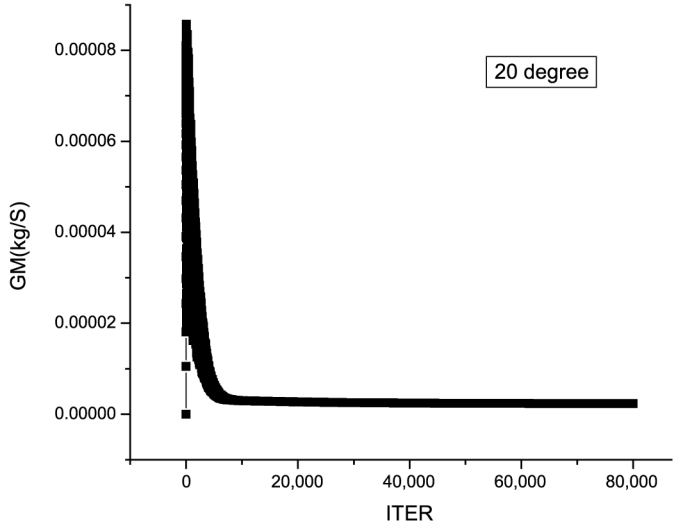

(b) $\theta = 20°$

(*continued*)

Figure 4.
GM vs iteration number for $\theta = 100°$-$180°$, and $\lambda_w = 10$ W/m K

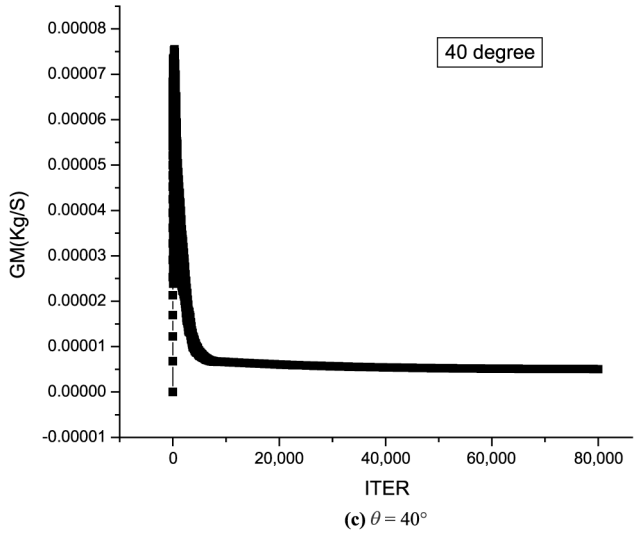

(c) $\theta = 40°$

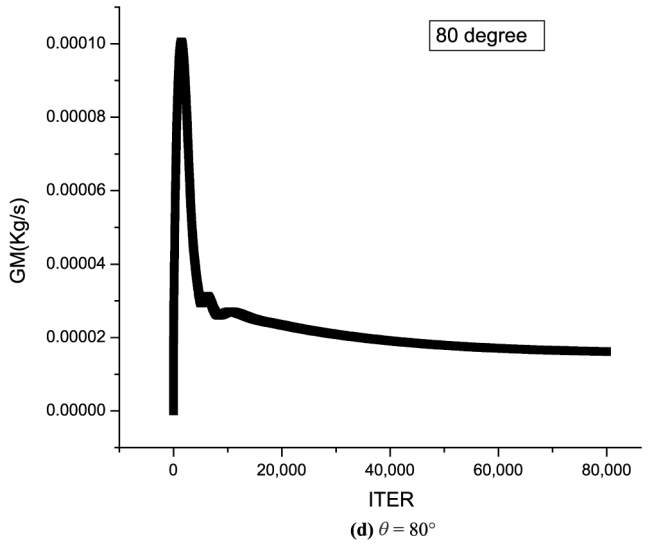

(d) $\theta = 80°$

Figure 4.

(3) SMAX/GM $\leq 1 \times 10^{-6}$

(4) ABS(SSUM/GM) $\leq 1 \times 10^{-7}$

In the above expressions SMAX is the absolute maximum value of control volume mass flow rate residual:

$$\text{SMAX} = \max\left[\text{abs}(F_{\text{w}} - F_{\text{e}} + F_{\text{s}} - F_{\text{n}})_{i,j,k}\right] \tag{8}$$

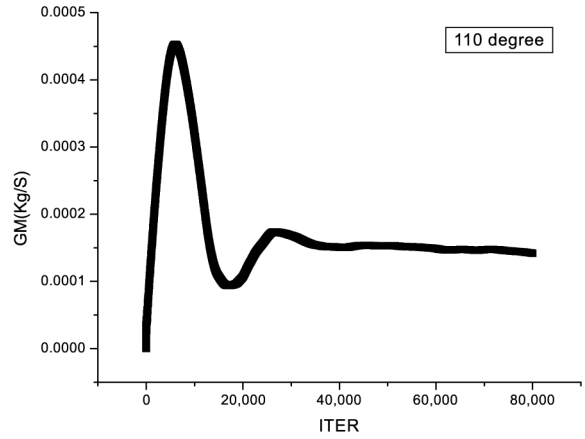

(a) $\theta = 110°$

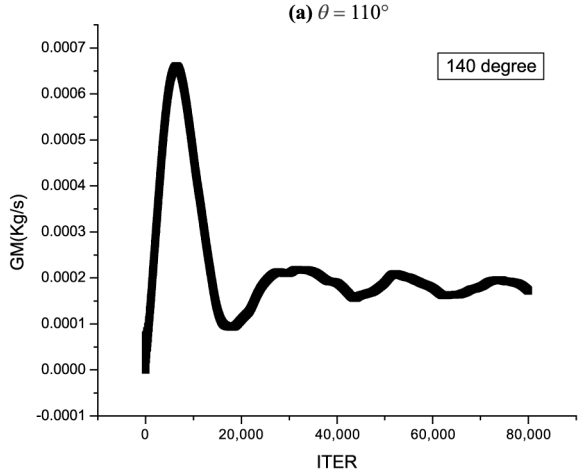

(b) $\theta = 140°$

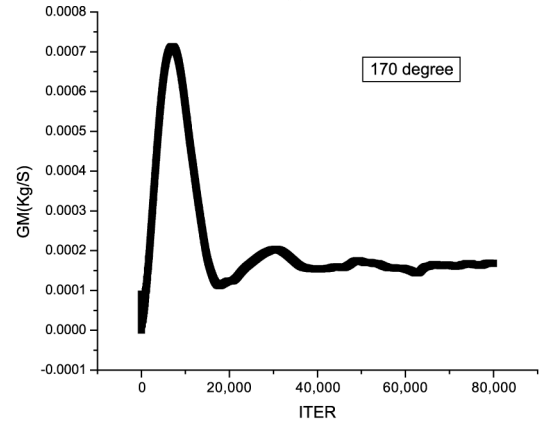

(c) $\theta = 170°$

Figure 5.
GM vs iteration number for $\theta = 100°$-$180°$, and $\lambda_w = 0.25$ W/m K

where F_e, F_w, F_n and F_s are the mass flow at the east, west, north and south interface of control volume (i,j,k), respectively. While SSUM is the summation of the mass flow rate residual of the whole computation domain:

$$\mathrm{SSUM} = \sum_{i,j,k} (F_w - F_e + F_s - F_n)_{i,j,k} \tag{9}$$

4. Results and discussion

4.1 Model and numerical methods validation

The code used in the present study is an extension of the code developed in He (2002), where the cylindrical wall was assumed being very thin and treated as adiabatic. Comprehensive code verification was conducted in He (2002), and a detail description was provided in He *et al.* (2004a). Thus, to save space such presentation is omitted. However, to verify the present model and code, two preliminary computations are conducted. First, the thermal conductivity of the tube wall was assumed to be 1.0×10^{-5} W/m K to simulate the situation of neglecting heat conduction in the lateral wall. Partial predicted results are presented in Table II, where the numerical results of He (2002) and He *et al.* (2004b) were also presented. In the table, the quantity Q_{cond} is the heat transfer rate of the heat transfer process in the envelope of heat conduction through the gas and tube wall from the hot to cold end. From the table, we see that the presented results are almost identical to that of He (2002) and He *et al.* (2004b), in which the thermal conductivity of the tube wall was totally neglected. The second computation was conducted for the inclined angle of 90°, i.e. the natural convection of helium in a horizontal cylindrical envelope. As indicated above, Kimura and Bejan (1980) once performed experiments for water in a horizontal cylindrical envelope. The thermal boundary conditions of their test are identical to our situation, with difference in working fluid, temperature difference and the dimensions. Since we could not get exact data of their test, for example, what is the thermal conductivity of the tube wall, we did not simulate their situation. Rather, we performed numerical experiments according to our condition. The thermal conductivity of the tube wall is taken as 0.25 W/m K. We believe that qualitatively the predicted results should have something in common compared to their experimental results. In Kimura and Bejan (1980) the temperature distributions along the diameter in five cross sections (one in the center, two adjacent to the hot and cold ends, and other two in between) and the top, center and bottom temperatures in the vertical longitudinal sections were provided. Our results of

Case	Q_m (W)	GM (kg/s)	Q_{cond} (W)
$\theta = 40°$			
$\lambda_w = 1.0 \times 10^{-5}$ W/m K	8.806×10^{-2}	2.937×10^{-6}	2.945×10^{-2}
Results in Bejan and Tien (1978)	8.860×10^{-2}	2.936×10^{-6}	2.945×10^{-2}
$\theta = 120°$			
$\lambda_w = 1.0 \times 10^{-5}$ W/m K	7.193	5.485×10^{-5}	2.779×10^{-2}
Results in Bejan and Tien (1978)	7.221	5.404×10^{-5}	2.782×10^{-2}
$\theta = 170°$			
$\lambda_w = 1.0 \times 10^{-5}$ W/m K	5.406	5.020×10^{-5}	2.784×10^{-2}
Results in Bejan and Tien (1978)	5.407	5.165×10^{-5}	2.788×10^{-2}

Table II.
Comparison of the presented results with that in work of He (2002) and He *et al.* (2004a, b)

temperature distributions are shown in Figures 6 and 7. It can be found that the present results of temperature distributions show very similar variation patterns to that shown in Figures 3 and 4 of Kimura and Bejan (1980). The axial velocity distributions are presented in Figure 8. It can be compared with Figure 8 in Kimura and Bejan (1980). Qualitatively, our numerical predictions of axial velocity agree well with that of Kimura and Bejan (1980), with difference mainly in the center part of the cylindrical space. For the water case shown in Kimura and Bejan (1980), there is a quite large portion of the cross section (about 50 per cent) where the axial velocity is near zero, with two opposite jets in the upper and lower parts of the cylinder. Our results show a gradual variation from top maximum value to the lower negative maximum value with a very small portion of zero axial velocity. We believe that this difference is mainly caused by the difference in Ra number (2.1×10^7 of the present case vs 1.78×10^9 of Kimura and Bejan (1980)) and different variation patterns of thermal physical properties with temperature.

The above two preliminary computations give some supports to the correctness and feasibility of the present model and numerical methods.

4.2 Heat transfer rate under different inclination angles

Computational results for the average heat transfer rate in the envelope are summarized in Tables III and IV for tube wall thermal conductivity of 10 and 0.25 W/m K, respectively. In these tables, Q_m is the average heat transfer rate of the cold and hot ends. Q_{cond} is the conduction heat transfer rate by assuming that the heat transfer process in the envelope were pure heat conduction through the gas and tube wall from the hot end to the cold end with the same end temperature difference; Ra_L, Ra_D are the Rayleigh numbers with envelope length and diameter as their characteristic length, respectively. All the fluid thermophysical properties in the calculation of Q_m, Q_{cond}, Ra_L and Ra_D were volume average ones.

To show the effect of the inclination angles and the wall thermal conductivity on the heat transfer rate more clearly, the variation of Q_m vs θ with different wall material is shown in Figure 9(a), where the results of He (2002) and He *et al.* (2004b) are also presented. Figure 9(b) is a copy from Thummes *et al.* (1997) where the natural convection for a pulse tube refrigerator was estimated from the measured cooling power. By comparing Figure 9(a) and (b) it can be seen that our numerical prediction of the variation pattern of heat transfer rate with inclination angle agree well with Thummes *et al.* (1997). This comparison gives a further support to the present model. From Tables III and IV and Figure 9(a) we see that the thermal conductivity of the wall has a great effect on the natural convection. When the material thermal conductivity is 0.25 W/m K, the greatest heat transfer rate is 7.824 W (occurs at $\theta = 120°$). When the material thermal conductivity is 10.0 W/m K, the greatest heat transfer rate is 10.89 W (occurs also at $\theta = 120°$). According to He (2002) and He *et al.* (2004b) when the wall heat conduction is neglected the highest heat transfer rate is 7.22 W (occurs at $\theta = 120°$). It can be seen clearly that the heat transfer rate from the hot end to the cold end is appreciably enhanced for a tube with higher thermal conductivity. Thus, as expected in He (2002) the negative deviation of the predicted heat transfer rate in He (2002) and He *et al.* (2004b) can be mainly attributed to the neglecting of the effect of the wall heat conduction, indeed. In Table V, comparisons are made between the results with different tube wall thermal conductivity. In the table, ΔQ_m is the increased amount of the mean heat transfer rate over the result neglecting the wall heat

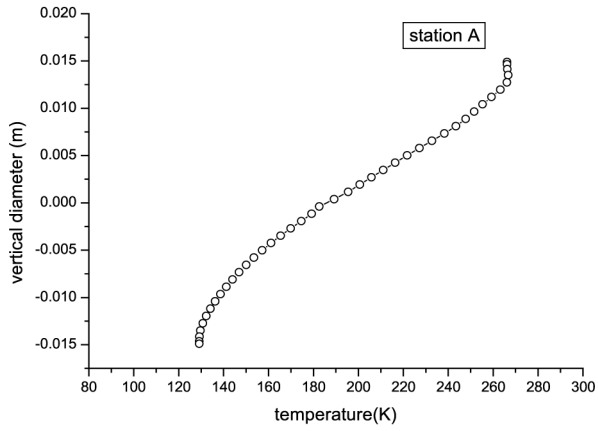

(a) z=0.011m

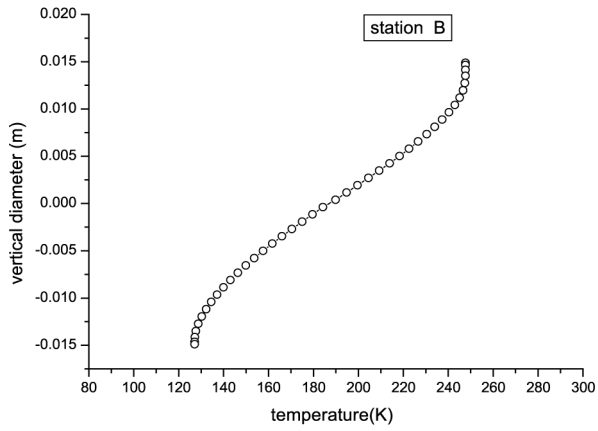

(b) z=0.059m

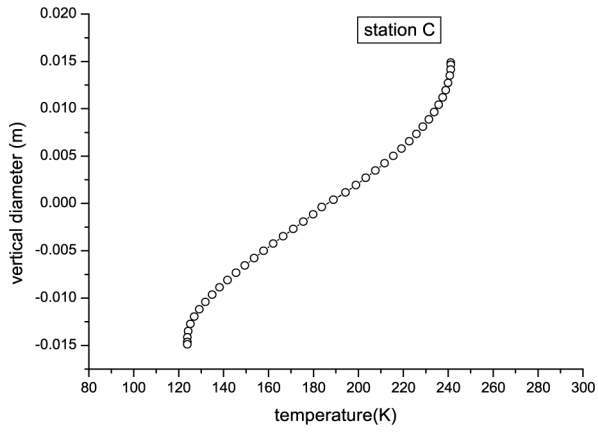

(c) z=0.119m

Figure 6.
Temperature distribution along the vertical diameter ($Ra = 1.884 \times 10^7$)

(*continued*)

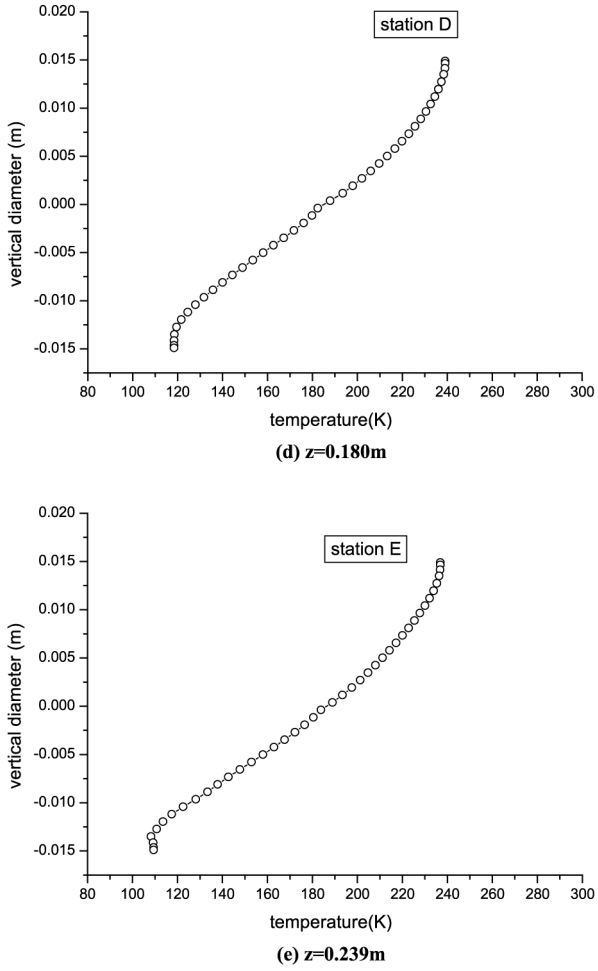

Figure 6.

conduction (He, 2002; He *et al.*, 2004b), and ΔQ_{cond} is the increased amount of the pure heat conduction along the tube wall. It can be seen that ΔQ_{cond} is almost a constant for different orientation, around 0.01 W for $\lambda_{\mathrm{w}} = 0.25\,\mathrm{W/m\,K}$ and around 0.4 W for $\lambda_{\mathrm{w}} = 10\,\mathrm{W/m\,K}$, while ΔQ_{m} increases rapidly with the increase in inclined angle and its values are much larger than the former, except for the zero degree case. This comparison reveals that the increase in the heat transfer rate in the envelope is mainly not from the heat conduction in the tube, but some enhancement in the convection must be induced. This will be analyzed in a later presentation.

In order to find the further effect of larger thermal conductivity, computation are conducted for four more cases with wall thermal conductivity of 30, 60, 100 and 200 W/m K, respectively. All the results of the total heat transfer rate are shown in Figure 10, where the wall thermal conductivity is taken as the abscissa. It can be seen that up to wall thermal conductivity $\lambda_{\mathrm{w}} = 60.0\,\mathrm{W/m\,K}$, the increase in the wall

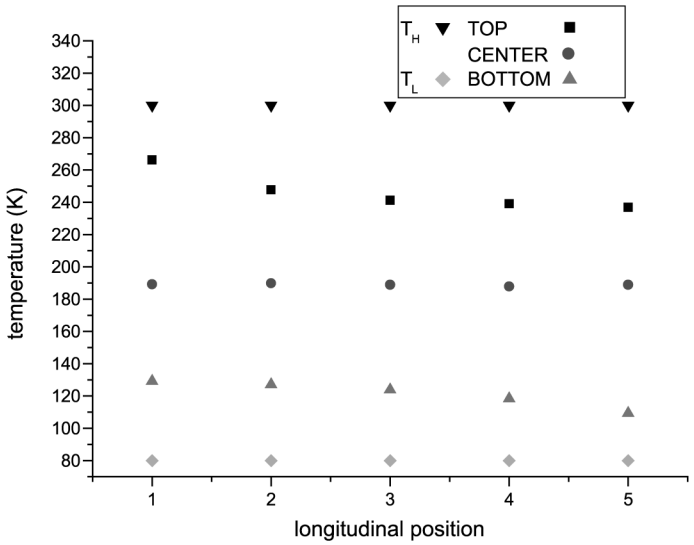

Figure 7.
Top, center and bottom temperature variation with longitudinal position ($Ra = 1.884 \times 10^7$)

thermal conductivity lead to the decrease of the curve slope. However, further increase in the wall thermal conductivity leads to almost a linear increase of the heat transfer rate, and there seems no limit of the wall thermal conductivity, beyond which further increase in it will not have a significant effect on the heat transfer rate. Such results can be understood as follows. Within the range of $\lambda_w \leq 60.0\,W/m\,K$, the increase in λ_w leads to both intensification of natural convection and heat conduction in the wall. The larger the wall thermal conductivity, the more important is the wall heat conduction in the total heat transfer rate from the hot end to the cold end. Thus, the natural convection takes less and less part of the total heat transfer rate with the increase in the wall thermal conductivity, and the slope of the curve Q-λ_w becomes smaller and smaller. When the wall thermal conductivity is larger than 60 W/m K, the wall heat conduction dominates compared with the natural convection, leading to almost linear increase in the heat transfer rate with λ_w. Thus, for the situation studied there seems no upper limit of the wall thermal conductivity beyond which further increase in λ_w will not have significant effect on the heat transfer rate. Since in the engineering application, stainless steel is the typical metal used for pulse tube, in the following presentation, only results for $\lambda_w = 10.0\,W/m\,K$ are provided in detail.

A numerical simulation for $\theta = 120°$ and $\lambda_w = 10.0\,W/m\,K$ by adopting Boussinesq assumption was also conducted. In the computation, the reference temperature was taken as t_c. The predicted heat transfer rate is 8.71 W which is 20 per cent lower than the result presented in Table III (10.89 W). This computation demonstrates the necessity of adopting the present model.

It is worth noting that the major purpose of this study is to reveal qualitatively the effect of the tube wall heat conduction on the characteristics of the natural convection in the long cylindrical envelope with different inclined angles. The major non-dimensional quantities are Rayleigh and the major result is the relative variation in heat transfer rate. Its absolute value is not so important. Furthermore, for the flow and temperature fields, only their patterns are important and the absolute values are of less importance.

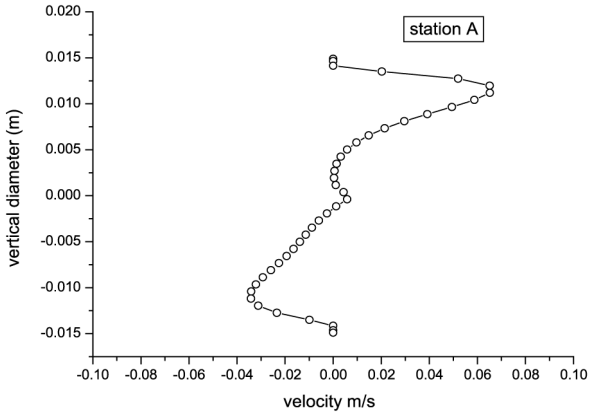

(a) z=0.011m

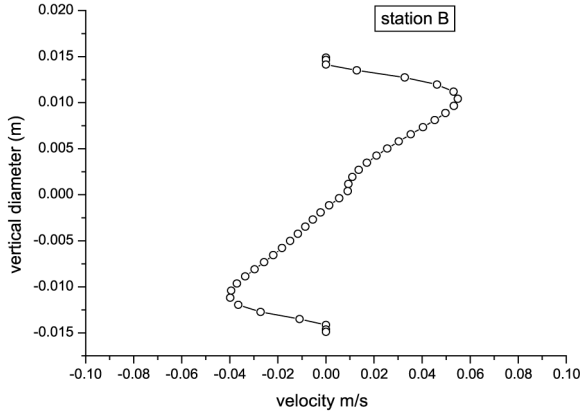

(b) z=0.059m

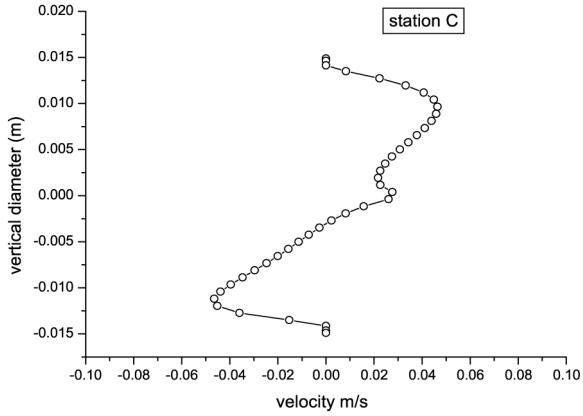

(c) z=0.119m

(*continued*)

Figure 8.
Axial velocity distribution along the vertical diameter ($Ra = 1.884 \times 10^7$)

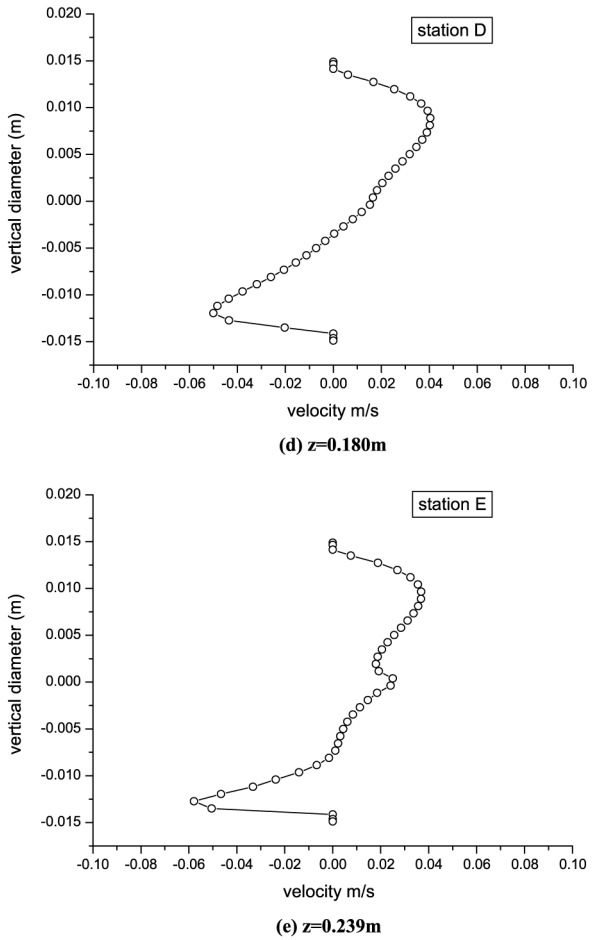

Figure 8.

Therefore, all the results of velocities and temperatures will be presented in dimensional way and no attempt was made to make them dimensionless. Although the specific values of the heat transfer rate, velocity and temperature predicted in this paper only apply to the case studied, since the value of Ra in the present computation is a typical one for the pulse tube refrigerator, the physical mechanism revealed, however, can also be applied to the same category of problems.

4.3 Natural convection enhancement due to tube wall heat conduction

As indicated above in the inclination angle range of 80°-180°, the increased amount of the heat transfer rate Q_m is much lager than the increased amount of the pure conduction Q_{cond}, while in the range of 0°-80°, the increased amount of heat transfer rate Q_m is very close to the increased amount of pure conduction Q_{cond}. That means when the hot end is down the effect of the wall heat conduction enhances heat transfer mainly not by the wall heat conduction itself, but by the enhancement of natural convection in the envelope. The reason of such enhancement is analyzed as follows.

θ°	$Ra_L \times 10^{-10}$	$Ra_D \times 10^{-7}$	GM (kg/s)	Q_m (W)	Q_{cond} (W)
0	1.578	2.165	5.286×10^{-8}	4.275×10^{-1}	4.271×10^{-1}
10	1.576	2.162	1.349×10^{-6}	4.352×10^{-1}	4.272×10^{-1}
20	1.575	2.160	2.977×10^{-6}	4.545×10^{-1}	4.272×10^{-1}
30	1.574	2.159	4.773×10^{-6}	4.825×10^{-1}	4.272×10^{-1}
40	1.574	2.158	6.600×10^{-6}	5.237×10^{-1}	4.272×10^{-1}
50	1.573	2.157	8.640×10^{-6}	5.700×10^{-1}	4.272×10^{-1}
60	1.575	2.160	1.250×10^{-5}	6.177×10^{-1}	4.271×10^{-1}
70	1.579	2.166	1.572×10^{-5}	7.890×10^{-1}	4.271×10^{-1}
80	1.554	2.131	3.035×10^{-5}	1.208	4.271×10^{-1}
90	1.349	1.850	6.808×10^{-5}	5.524	4.271×10^{-1}
100	1.326	1.819	8.808×10^{-5}	8.644	4.270×10^{-1}
110	1.355	1.858	9.579×10^{-5}	10.12	4.269×10^{-1}
120	1.544	2.118	9.873×10^{-5}	10.89	4.264×10^{-1}
130	1.557	2.135	8.104×10^{-5}	10.82	4.263×10^{-1}
140	1.548	2.122	9.358×10^{-5}	10.49	4.263×10^{-1}
150	1.560	2.139	9.767×10^{-5}	10.12	4.263×10^{-1}
160	1.495	2.050	1.096×10^{-4}	9.970	4.265×10^{-1}
170	1.492	2.046	1.478×10^{-4}	9.736	4.265×10^{-1}
180	1.258	1.726	1.532×10^{-4}	9.211	4.272×10^{-1}

Table III.
Computational results for $\theta = 0^\circ - 180^\circ$, and $\lambda_w = 10\,W/m\,K$

θ°	$Ra_L \times 10^{-10}$	$Ra_D \times 10^{-7}$	GM (kg/s)	Q_m (W)	Q_{cond} (W)
0	1.564	2.145	4.230×10^{-8}	4.030×10^{-2}	3.936×10^{-2}
10	1.557	2.136	5.046×10^{-7}	4.884×10^{-2}	3.937×10^{-2}
20	1.552	2.129	1.240×10^{-6}	6.011×10^{-2}	3.939×10^{-2}
30	1.556	2.134	2.240×10^{-6}	7.181×10^{-2}	3.938×10^{-2}
40	1.567	2.148	3.215×10^{-6}	9.850×10^{-2}	3.936×10^{-2}
50	1.585	2.173	4.033×10^{-6}	1.381×10^{-1}	3.933×10^{-2}
60	1.610	2.208	4.625×10^{-6}	2.034×10^{-1}	3.928×10^{-2}
70	1.652	2.266	5.073×10^{-6}	3.364×10^{-1}	3.919×10^{-2}
80	1.666	2.285	6.456×10^{-6}	8.941×10^{-1}	3.908×10^{-2}
90	1.374	1.884	1.877×10^{-5}	5.095	3.919×10^{-2}
100	1.528	2.096	5.614×10^{-5}	7.336	3.875×10^{-2}
110	1.738	2.384	5.767×10^{-5}	7.549	3.817×10^{-2}
120	1.990	2.729	5.846×10^{-5}	7.824	3.763×10^{-2}
130	1.951	2.676	5.121×10^{-5}	6.984	3.767×10^{-2}
140	1.912	2.622	5.073×10^{-5}	6.598	3.773×10^{-2}
150	1.920	2.633	5.631×10^{-5}	6.398	3.765×10^{-2}
160	1.894	2.598	5.117×10^{-5}	5.854	3.770×10^{-2}
170	1.785	2.448	5.909×10^{-5}	5.281	3.789×10^{-2}
180	1.438	1.972	6.444×10^{-5}	4.719	3.878×10^{-2}

Table IV.
Computational results for $\theta = 0^\circ - 180^\circ$ and $\lambda_w = 0.25\,W/m\,K$

The variation of the cross section average temperature with axial position is shown in Figure 11(a). Three kinds of averaged temperatures are shown in the figure: the mean values of the whole cross section (represented by square), the mean values of tube wall (triangle), and the mean value of the gas section (circle). Following features may be noted. First, in the most part of the envelope the three kinds of mean temperatures vary almost linearly along the tube axis, while in

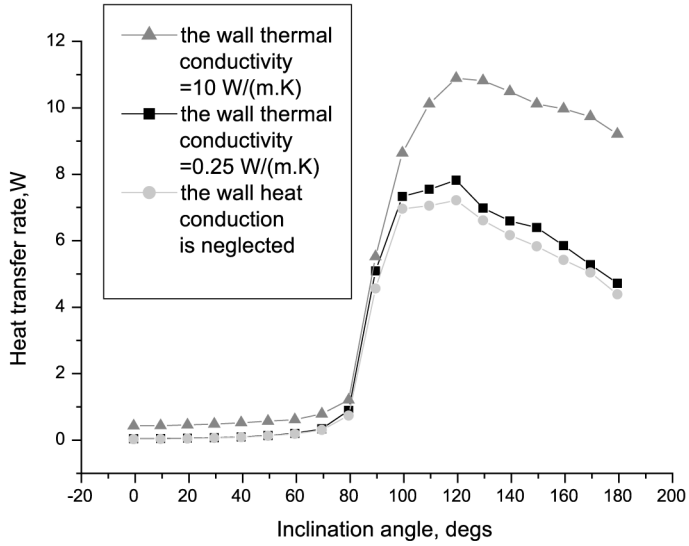

(a) Predicted heat transfer rate (*L/d*=9, *d*=27.8 mm)

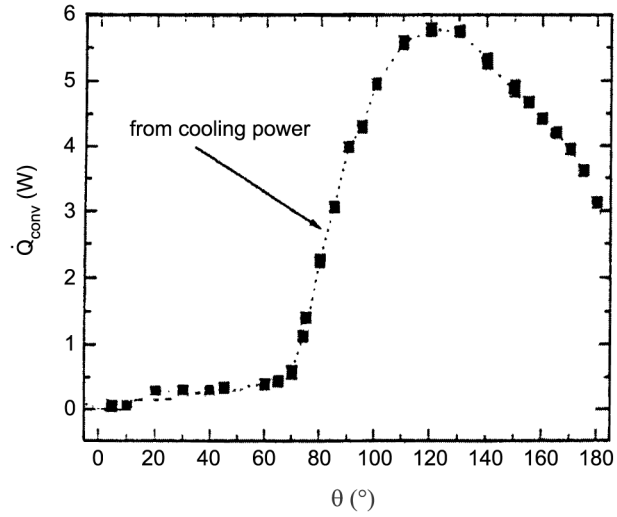

(b) Estimated from cooling power (*L/d*=18.7, *d*=13.4 mm) [18]

Figure 9.
Variation of heat transfer rate with different inclination angle and different material of the lateral wall

a very narrow region near the two ends, the temperatures vary very rapidly. This means that near the two ends, there is a large amount of heat conducted from wall to the gas (at hot end) or from the gas to the wall (at cold end). Second, in almost half length of the envelope the wall temperature is much higher than the average gas temperature at the same axial location, while in the other half length of the envelope, the situation is the opposite. This cross sectional temperature difference

between the wall and the gas may cause secondary convection in the fluid. It is this enhanced convection that augments the heat transfer in the envelope: in the half envelope adjacent to the hot end, the tube wall receives energy from the hot end by conduction and then transfers most part of the energy to the fluid, while in the other half of the envelope the tube wall with lower temperature receives energy from fluid and transfers the energy to the cold end by conduction. In such a way, the total natural convection heat transfer rate is greatly enhanced. Third, the average gas temperature in the half envelope adjacent to the cold end is higher than that adjacent to the hot end. This temperature distribution pattern of gas seems abnormal. However, if we consider that there is a global circulation between the hot and cold ends and temperature reverse is an inherent character for the

Case	ΔQ_m (W)	ΔQ_{cond} (W)
Tube wall thermal conductivity = 0.25 W/m K		
0°	0.0107	0.0099
80°	0.1541	0.0100
120°	0.6030	0.0098
180°	0.3810	0.0104
Tube wall thermal conductivity = 10 W/m K		
0°	0.4027	0.3977
80°	0.5400	0.3980
120°	3.449	0.3993
180°	4.025	0.3991

Table V.
Comparison of heat transfer rate with different tube wall thermal conductivity (thickness of tube wall, $\delta = 1$ mm)

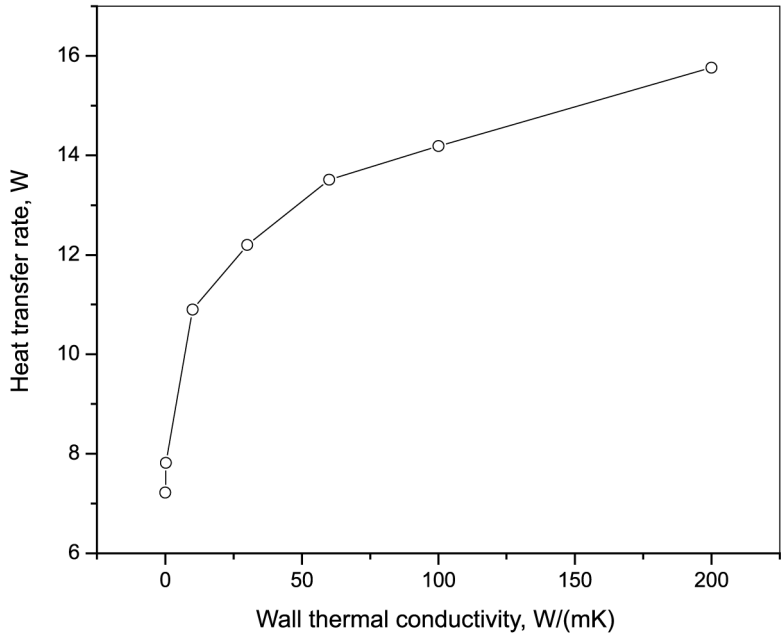

Figure 10.
Variation of total heat transfer rate with wall thermal conductivity

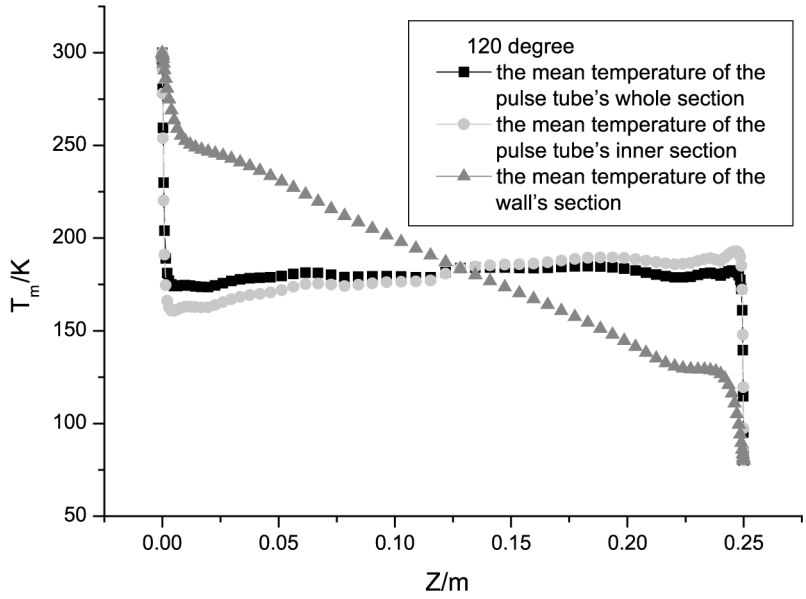

(a) Axial distribution of average fluid temperature

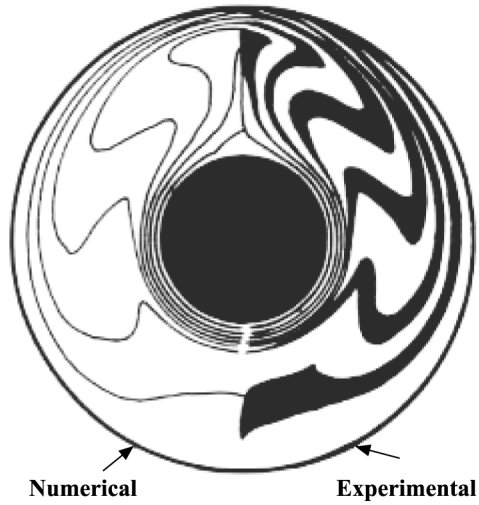

(b) Isothermals of natural convection in an annulus [1]

Figure 11.
Axial distribution of section average temperature for $\theta = 120°$ and $\theta = 180°$, and $\lambda_w = 10\,W/mK$

convection-dominated regime of natural convection in an enclosure, such a distribution pattern is understandable. This variation pattern is similar to the S-type isothermals (temperature reverse) of natural convection in annulus. For comparison, the results of Kuehu and Goldstein (1976) is shown in Figure 11(b),

where the S-type isothermals can be clearly observed. The S-type isothermals indicate that in the "S" region fluid temperature at the location near the hot wall is lower than the fluid temperature at the location near the cold wall. The existence of the S-type isothermals is a feature common to the natural convection in enclosure when convection is dominated (Barakos and Mitsoulis, 1994; Ozoe *et al.*, 1985; Wei and Tao, 1996a, b), and this does not violate the second law of the thermodynamics. This is because there is a big temperature difference between the two end walls, and it is this big temperature difference that causes the flow from the hot end to the cold end.

The enhancement of the natural convection due to tube wall heat conduction can also be revealed from the value of GM. As indicated earlier, the physical meaning of GM is the section-averaged axial flow rate. Obviously, for the same orientation, the larger the value of GM, the strong the natural convection in the enclosure. The section-averaged axial flow rate GM with different tube materials and orientations are presented in Table VI. We can infer from the table that the tube wall thermal conductivity has great effect on the section-averaged flow rate. The larger the tube wall thermal conductivity, the larger the section-averaged flow rate, and hence the natural convection.

From Tables III and IV, it can be seen that the orientation of $\theta = 120°$ has the maximum heat transfer rate between the hot and cold ends, therefore, the following presentations for velocity and temperature distributions will only be given for this orientation. The enhanced natural convection by wall conduction will be further demonstrated in the presentation for velocity and isothermal contours.

4.4 Velocity distributions for 120° orientation

A general view of the velocity distribution in the longitudinal cross section across the axis of the envelope is shown in Figure 12. For the purpose of clarity, the picture is not drawn in scale. To see the flow direction more clearly, the local velocity vectors near the hot and cold ends are magnified and shown in Figure 13. In Figures 12 and 13, the orientation of the envelope is positioned as it is. In Figure 13, the cross-sectional view of the velocity vectors are presented for nine sections. For these computations, the tube wall thermal conductivity is 10 W/m K.

It can be clearly seen from Figures 12 and 13 that there is a global clockwise circulation within the envelope: heated fluid goes from hot end upward in the lower part of the envelope, and cooled fluid goes downward in the upper part of the envelope. Hence, along the hot end fluid moves downward, while along the cold end the fluid moves upward. And because of this global circulation, velocity vectors in the mid region around $r = 0$ appear to be separated: in the upper half and lower half of

Table VI. Variation of the cross-sectional axial flow rate GM with thermal conductivity and orientations

	$\theta°$ GM (kg/s)				
Case	40	80	120	140	180
Neglecting wall heat conduction	2.936×10^{-6}	5.687×10^{-6}	5.404×10^{-5}	4.531×10^{-5}	8.739×10^{-5}
$\lambda_w = 0.25$ W/m K	3.215×10^{-6}	6.456×10^{-6}	5.846×10^{-5}	5.073×10^{-5}	6.444×10^{-5}
$\lambda_w = 10.0$ W/m K	6.600×10^{-6}	3.035×10^{-5}	9.873×10^{-5}	9.358×10^{-5}	1.532×10^{-4}

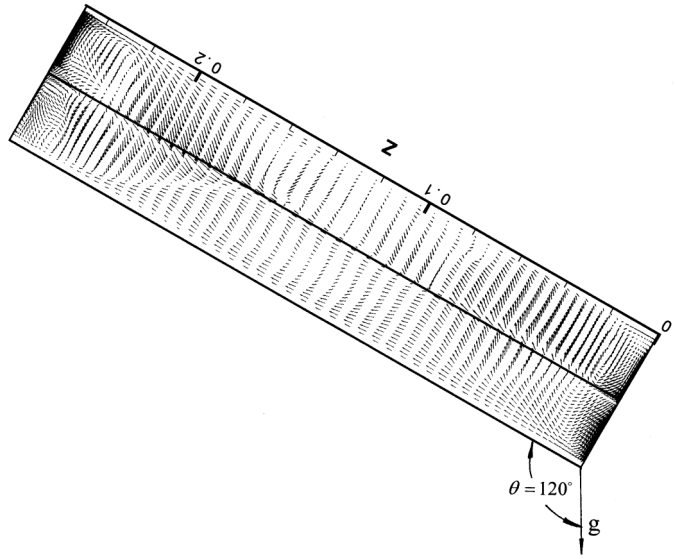

Figure 12.
Velocity vector in longitudinal section for $\theta = 120°$, and $\lambda_w = 10$ W/m K

the enclosure, the velocity vectors have opposite directions. Near the hot and cold ends there are two regions where velocity vectors seem abnormal: near the hot end in the upper part some fluid goes upward, while near the cold end in the lower part some fluid goes downward. Actually, in these two local regions the secondary convection induced by the temperature difference between the tube wall and fluid occurs, and this is shown in Figure 14. From the velocity field of each cross section shown in Figure 14 it can be observed that each cross section has at least one vortex, indicating that the flow structure in such an envelope is a multiple-vortex one. From Figure 14(a)-(c) and (g)-(i) we find that near the two ends, the velocity adjacent to the lateral wall is comparatively greater than the inner part of the fluid. The relatively high velocity of the fluid adjacent to the lateral wall is the indication of an intensified local natural convection in that region, which is caused by the big temperature difference between the wall and the fluid. To show the enhanced natural convection due to the tube wall heat conduction, two special comparisons are made, and are shown in Figure 15. In Figure 15(a) and (b), the velocity distributions in cross-sections with $z = 0.011$ and 0.239 m are shown, respectively. In each pair of pictures, one is the result obtained without considering the wall heat conduction, while the other is the outcome of wall heat conduction. It can be seen clearly that in the results with wall heat conduction, the circumferential velocity near the cylindrical surface is appreciably larger than that without wall heat conduction. In addition, near the hot end the secondary convection stream goes upward because of the heating of the fluid and near the cold end the secondary flow moves downward because of cooling effect. The enhanced circumferential fluid flow certainly makes contribution to the enhancement of heat transfer.

4.5 Temperature distributions of 120° orientation

In Figure 16, the isothermal contours in the longitudinal section is shown. To see the isothermal contours more clearly, the local isothermal contours near the hot and cold ends

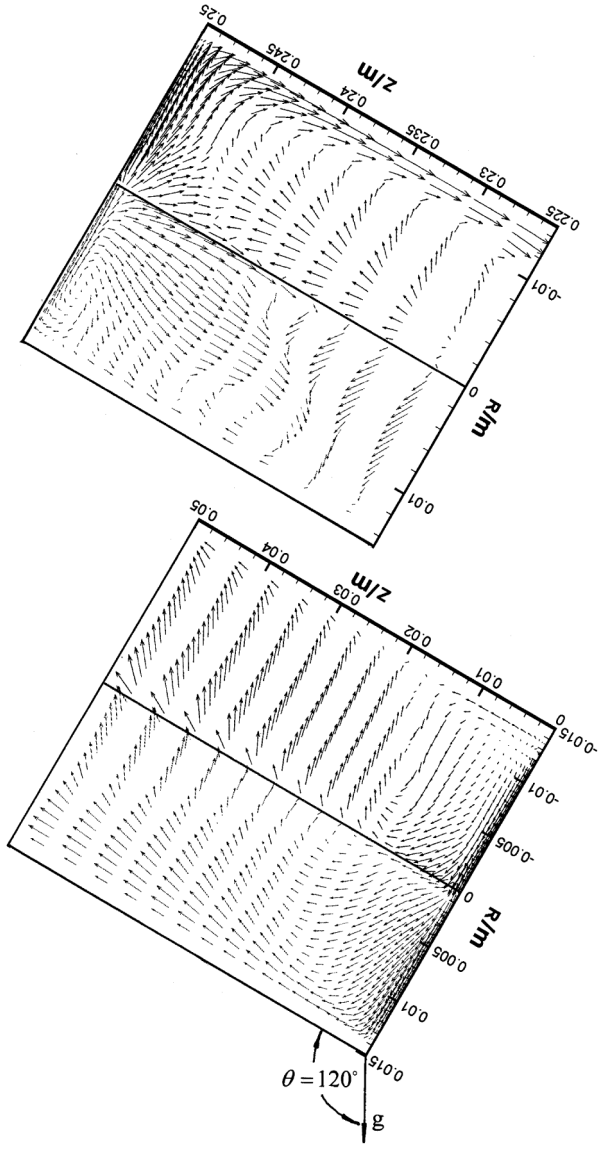

Upper: Local velocity field near cold end
Lower: Local velocity field near hot end

Figure 13.
Details of the flow pattern in longitudinal section for $\theta = 120°$, and $\lambda_w = 10$ W/m K

are magnified and shown in Figure 17. Figure 18 shows the isothermals in nine transverse sections. For these computations, the tube wall thermal conductivity is 10 W/m K.

In the longitudinal section temperature contours seem very complicated. Near the cold end an isothermal contour with a high temperature of 203.75 K can be found, while

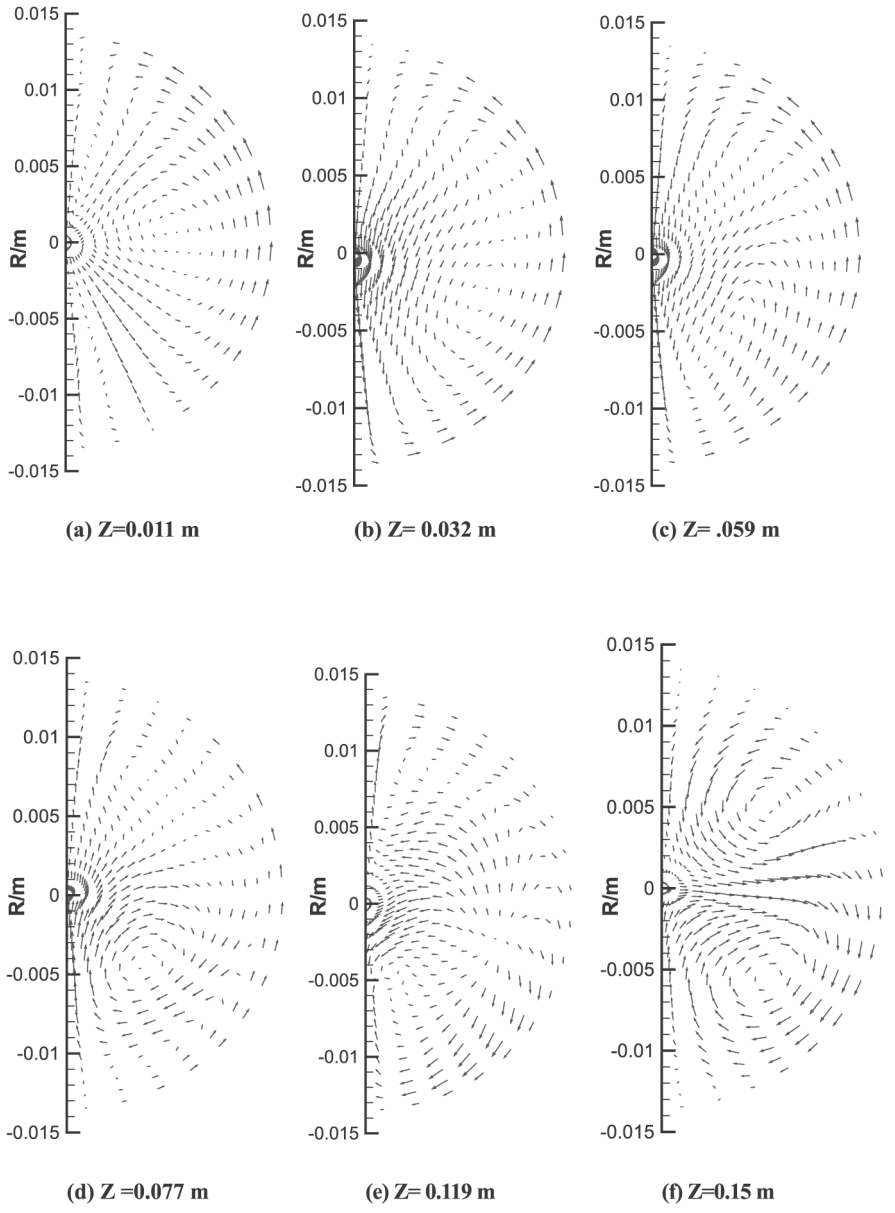

Figure 14.
Cross section velocity distribution for $\theta = 120°$, and $\lambda_w = 10$ W/m K

(*continued*)

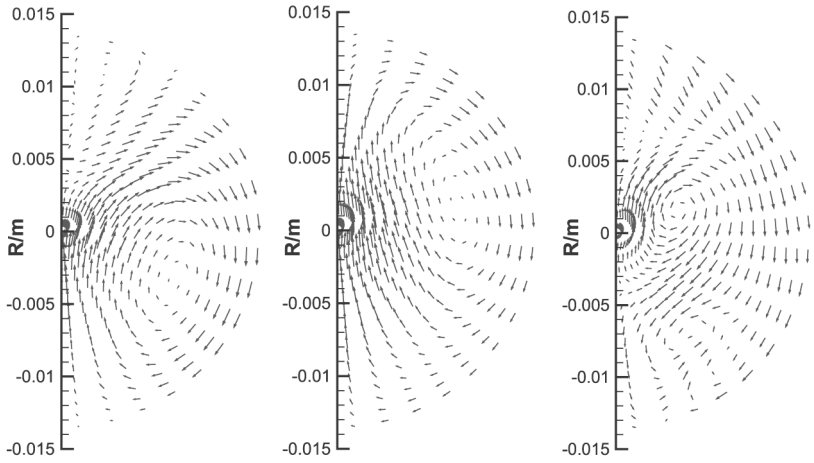

Figure 14.

near the hot end there exists a low temperature contour of 162.5 K. From the temperature distributions in the vicinity of the hot and cold ends, very steep change of fluid temperature can be found (Figure 17): within a thin layer about 1 mm the fluid temperature may increase from 80 to 201.304 K or decrease from 300 to 148.75 K This complicated temperature distribution is caused by the global convective flow and is consistent with the section averaged fluid temperature distribution discussed above. Another important feature of the temperature contours in the longitudinal section is that some isothermal lines are along the axial coordinate at $r = 0$. This is mainly caused by the global circulation of the fluid: in the upper part of the envelope fluid goes from hot to cold end; while in the lower part of the envelope, cooled fluid goes from cold to hot end. These two streams meet in the region around $r = 0$, resulting in the above-mentioned isothermal distribution.

The temperature distributions at nine cross sections are shown in Figure 18. The major characters of these contours are as follows. First, the fluid temperature in the upper part of each section is higher than that in the lower part, reflecting one of the basic features of natural convection in enclosures. Second, from Figure 18(a)-(d), which are near the hot end of the pulse tube, it can be observed that the isothermals adjacent to the solid wall are much denser than that of the inner part fluid. The same character can be observed from Figure 18(f)-(i) which are near the cold end of the tube. To show the intensified local convection between the wall and the adjacent fluid more clearly a comparison is made between the temperature contours for the cases with and without the wall heat conduction. The results are shown in Figure 19 for the two cross sections near the hot and cold ends. Figure 18 shows that for the case with wall heat conduction near the lateral surface there is a very dense isothermal distribution which is basically parallel to the wall surface, indicating enhanced heat transfer in the fluid. While for the case without the wall heat conduction, the isothermals intersect normally at the wall surface, reflecting an adiabatic boundary condition.

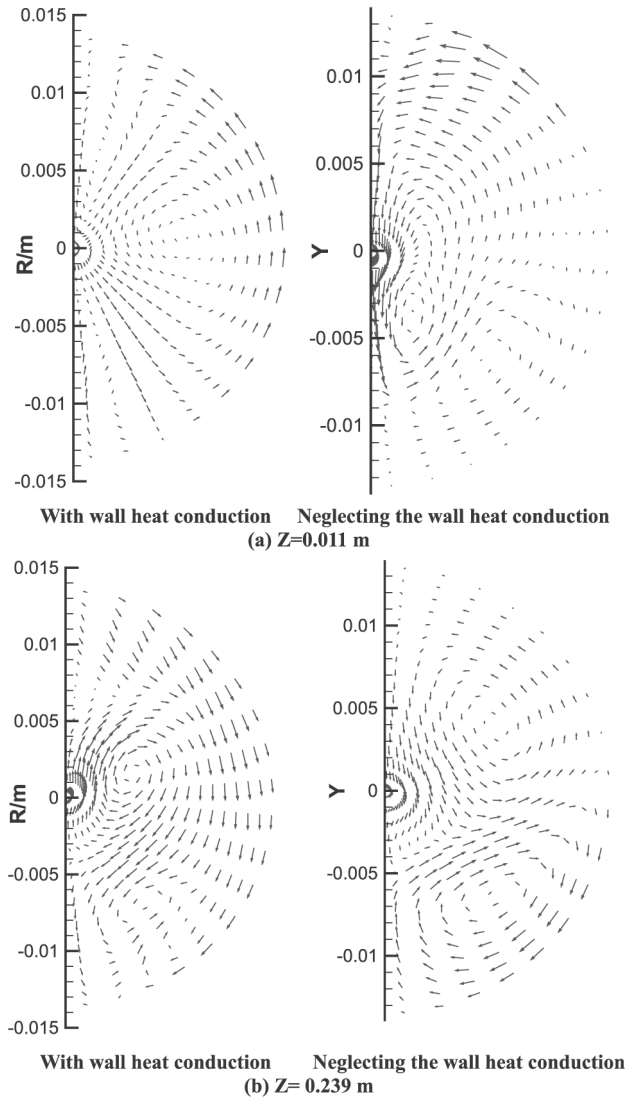

Figure 15.
Comparison of the cross section velocity distribution with and without wall heat conduction

4.6 Radiation heat transfer between the hot and cold ends

Since the temperature difference between the hot and cold ends is as high as 220 K, it is interesting to estimate the radiative heat transfer between the two ends, and compare it with the one by natural convection. The problem at hand may be modelled by an enclosed system with three surfaces: a hot surface, a cold surface and an adiabatic one. According to the heat transfer theory (Incropera and DeWitt, 1996), the net radiative heat transfer rate between the hot and cold ones may be determined by

$$Q = \frac{E_{bh} - E_{bc}}{\sum R_t} \tag{10}$$

where E_b is the black body emissive power, and R_t is the radiative thermal resistance. The summation of the radiative thermal resistance is

$$\sum R_t = \frac{1 - \varepsilon_h}{\varepsilon_h A_h} + \frac{1 - \varepsilon_c}{\varepsilon_c A_c} + R_{eq} \tag{11}$$

The equivalent thermal resistance is determined by

$$R_{eq} = \frac{1}{\frac{1}{A_h X_{h,c}}} + \frac{1}{\frac{1}{A_h X_{h,a}} + \frac{1}{A_c X_{c,a}}} \tag{12}$$

For the tube studied, we have:

$$A_h = A_c, \quad X_{h,a} = X_{c,a} \tag{13}$$

In addition, according to the characteristics of the angle factor, we have:

$$X_{h,c} + X_{h,a} = 1 \tag{14}$$

where $X_{h,c}$ only depends on the ratio L/d and can be calculated by

$$X = 0.5[S - (S^2 - 4)^{1/2}] \tag{15}$$

The parameter S is a function of L/d:

$$S = 1 + \frac{1 + (0.5d/L)^2}{(0.5d/L)^2} \tag{16}$$

Taking $T_h = 300\,K$, $T_c = 80\,K$, and $L/d = 6 - 20$, $\varepsilon = 0.05 - 0.8$, the radiative heat transfer rate between the hot and cold ends varies from 0.00611 to 0.0258 W.

The radiative heat transfer rate is in the order of, or even less than, pure heat conduction through the gas of the tube. Thus, it can be concluded that compared with natural convection, the radiative heat transfer rate between the hot and cold ends is trivial and may be neglected.

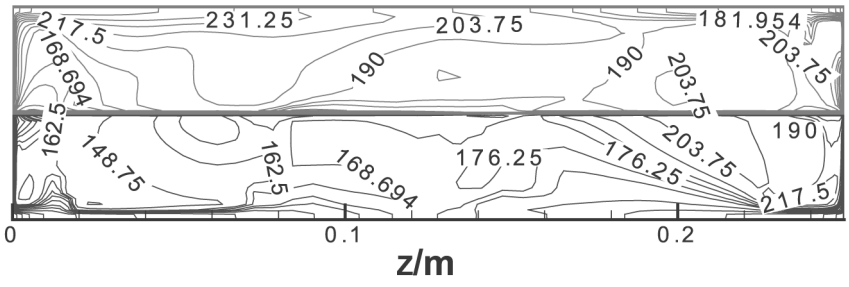

Figure 16.
Temperature contour in the entire longitudinal section for $\theta = 120°$, and $\lambda_w = 10$ W/m K

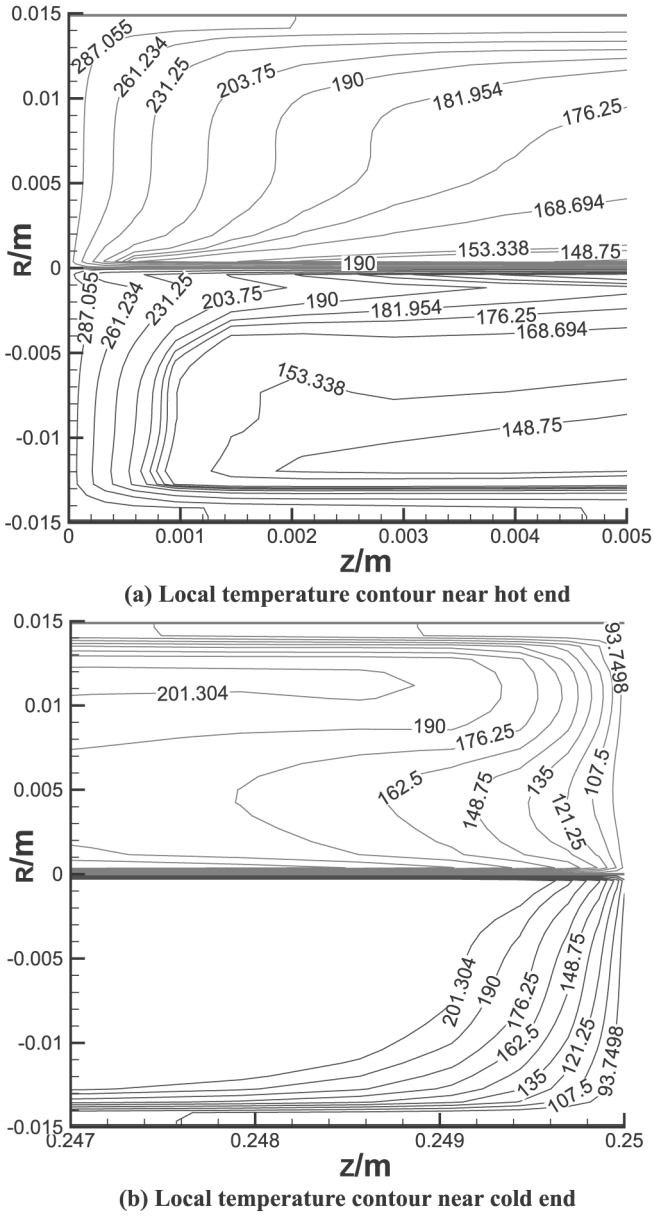

(a) Local temperature contour near hot end

(b) Local temperature contour near cold end

Figure 17.
Local isothermal contours for $\theta = 120°$, and $\lambda_w = 10\,W/m\,K$

5. Conclusions

The effect of the lateral wall heat conduction on the natural convection in a titled long cylindrical envelope with constant, but different temperature of the two end surfaces was numerically investigated. It has been demonstrated that:

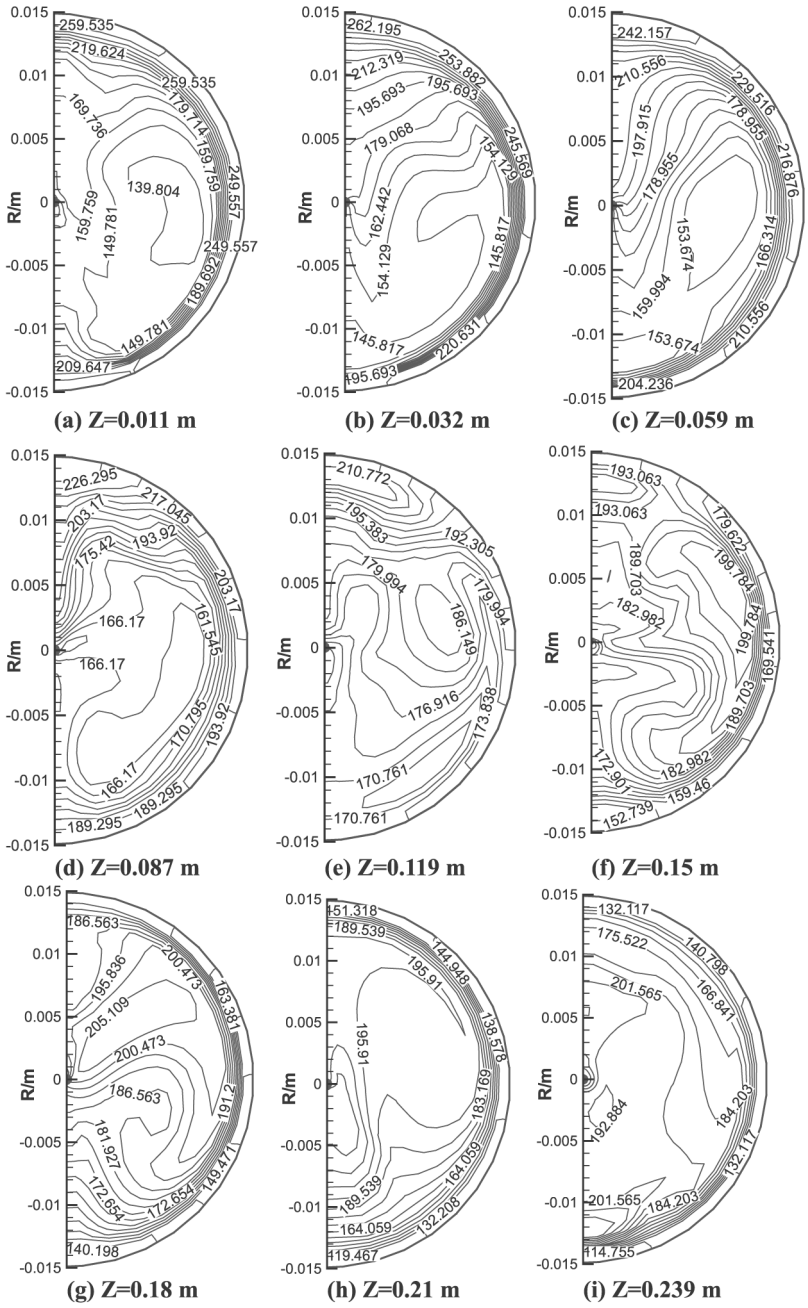

Figure 18.
Temperature contour in nine cross-sections for $\theta = 120°$, and $\lambda_w = 10$ W/m K

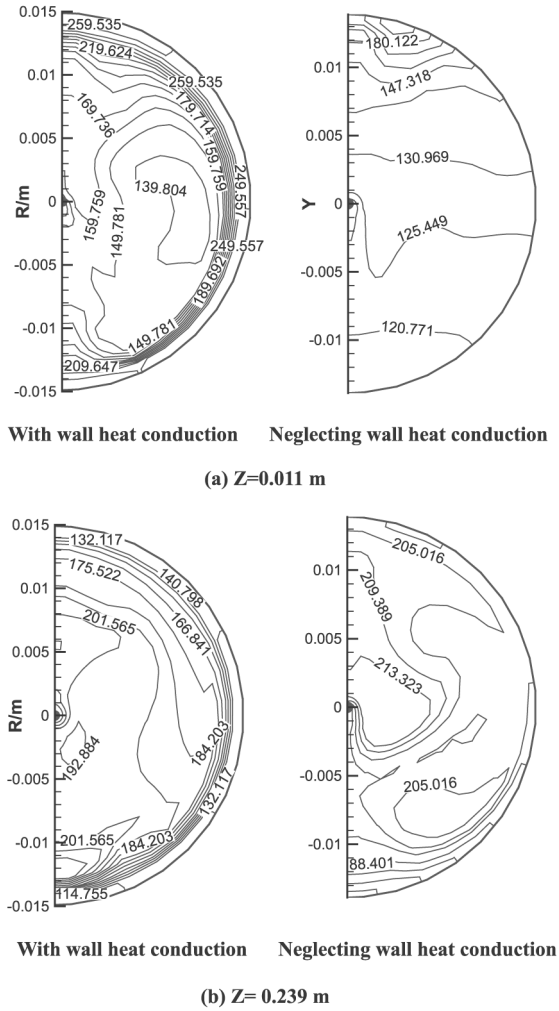

Figure 19.
Comparison of the cross section temperature distribution with and without wall heat conduction

(1) The heat transfer rate from hot to cold end of the enclosure with lateral wall heat conduction is higher than that neglecting the wall heat conduction. The enhancement amount of heat transfer rate is usually greater than that enhanced by the pure heat conduction in the wall only.

(2) When the tube is positioned at an inclination angle range from 0° to 80°, the effect of the lateral wall heat conduction on natural convection is limited because natural convection is weak in this range of inclination angle; while in the inclination angle range from 80° to 180°, the increased amount of natural convection heat transfer rate is much larger than the wall pure heat conduction.

(3) There exists a significant temperature difference between the wall surface and the fluid near the two ends when the tube wall heat conduction is condiered.

This great temperature difference causes an intensified local convection between the wall and the adjacent fluid, and this is the major reason why the heat transfer rate increased appreciably by considering the tube wall heat conduction. When the wall thermal conductivity is larger than a certain value, for the present case $\lambda_w = 60\,W/m\,K$, the natural convection plays a less important role in the total heat transfer from the hot to the cold end, and the heat transfer rate increases almost linearly with the increase in wall thermal conductivity.

(4) The radiative heat transfer rate between the hot and cold ends is at most in the order of the pure heat conduction through the gas in the tube, thus its effect on the cooling capacity loss may be neglected.

(5) To reduce the additional heat transfer from hot to cold ends via heat conduction mechanism of the wall, its thermal conductivity should be as low as possible.

References

Barakos, G. and Mitsoulis, E. (1994), "Natural convection flow in a square cavity revisited: laminar and turbulent models with wall function", *Int. J. Numer. Methods Fluids*, Vol. 18, pp. 695-719.

Barron, R.F. (1999), *Cryogenic Heat Transfer*, Taylor & Francis, New York, NY.

Bejan, A. and Tien, C.L. (1978), "Fully developed natural counterflow in a long horizontal pipe with different end temperatures", *Int. J. Heat Mass Transfer*, Vol. 21, pp. 701-8.

Charrie-Mojtabi, M.C., Mojtabi, A. and Caltagirone, J.P. (1979), "Numerical solution of a flow due to natural convection in horizontal cylindrical annulus", *ASME J. Heat Transfer*, Vol. 101, pp. 171-3.

Costa, V.A.F. (2002), "Laminar natural convection in differentially heated rectangular enclosures with vertical diffusive walls", *Int. J. Heat Mass Transfer*, Vol. 45, pp. 4217-25.

Date, A.W. (1986), "Numerical prediction of natural convection heat transfer in horizontal annulus", *Int. J. Heat Mass Transfer*, Vol. 29, pp. 1457-64.

De Vahl Davis, G. (1983), "Natural convection of air in square cavity", *Int. J. Numer. Methods Fluids*, Vol. 3, pp. 249-64.

Du, Z-G. and Bilgen, E. (1992), "Coupling of wall conduction with natural convection heat transfer in a rectangular enclosure", *Int. J. Heat Mass Transfer*, Vol. 35 No. 8, pp. 1969-75.

Edwards, D.K. and Catton, I. (1969), "Prediction of heat transfer by natural convection in closed cylinders heated from below", *Int. J. Heat Mass Transfer*, Vol. 12, pp. 23-30.

Gary, D.D. and Giorgin, A. (1976), "The validity of the Boussinesq approximation for liquids and gases", *Int. J. Heat Mass Transfer*, Vol. 19, pp. 545-51.

He, Y.L. (2002), "Theoretical and experimental investigations on the performance improvements of split-Stirling refrigerator and pulse tube cryocooler", PhD thesis, School of Energy and Power Engineering, Xi'an Jaiotong University, Xi'an, China.

He, Y.L., Tao, W.Q. and Chen, Z.Q. (2004a), "Natural convection in a tilted long cylindrical envelope with lateral adiabatic surface, part 1: theoretical modelling, numerical treatments and average heat transfer", *Numer. Heat Transfer, Part B* (in press).

He, Y.L., Tao, W.Q. and Chen, Z.Q. (2004b), "Natural convection in a tilted long cylindrical envelope with lateral adiabatic surface, part 2: heat transfer rate, flow patterns and temperature distributions", *Numer. Heat Transfer, Part B* (in press).

Ho, C.J. and Lin, Y.H. (1989), "Thermal convection heat transfer of air/water layers enclosed in horizontal annuli with mixed boundary conditions", *Warme-und Stoffubertragung*, Vol. 24, pp. 211-24.

Ho, C.J. and Lin, Y.H. (1990), "Natural convection of clod water in a vertical annulus with constant flux on the inner wall", *ASME J. Heat Transfer*, Vol. 112, pp. 117-23.

Ho, C.J., Lin, Y.H. and Chen, T.C. (1989), "A numerical study of natural convection in concentric and eccentric horizontal cylindrical annuli with mixed boundary conditions", *Int. J. Heat Fluid Flow*, Vol. 10, pp. 40-7.

Hortman, M. and Peric, M. (1994), "Finite volume multigrid prediction of laminar natural convection: benchmark solutions", *Int. J. Numer. Methods Fluids*, Vol. 18, pp. 695-719.

Incropera, F.P. and DeWitt, D.P. (1996), *Introduction to Heat Transfer*, 3rd ed., Wiley, New York, NY, pp. 690-708.

Kays, W.M. and Crawford, M.E. (1980), *Convective Heat and Mass Transfer*, 2nd ed., McGraw-Hill, New York, NY, p. 315.

Keyhani, M., Kulacki, F.A. and Christensen, R.N. (1983), "Free convection in a vertical annulus with constant heat flux on the inner wall", *ASME J. Heat Transfer*, Vol. 105, pp. 454-9.

Kim, D.M. and Viakanta, R. (1985), "Effect of wall heat conduction on natural convection heat transfer in a square enclosure", *ASME J. Heat Transfer*, Vol. 107, pp. 139-46.

Kimura, S. and Bejan, A. (1980), "Experimental study of natural convection in a horizontal cylinder with different end temperatures", *Int. J. Heat Mass transfer*, Vol. 23, pp. 1117-26.

Kuehn, T.H. and Goldstein, R.J. (1976), "An experimental and theoretical study of natural convection in the annulus between horizontal concentric cylinders", *J. Fluid Mech.*, Vol. 74, pp. 605-719.

Kuehn, T.H. and Goldstein, R.J. (1980), "A parametric study on Prandtl number and diameter ratio effects on natural convection heat transfer in horizontal cylindrical annulus", *ASME J. Heat Transfer*, Vol. 102, pp. 768-70.

Lankhorst, A. (1991), "Laminar and turbulent natural convection in cavities: numerical modeling and experimental validation", PhD thesis, Delft University of Technology.

Ozoe, H., Mouri, A., Ohmoro, M., Churchill, S.W. and Lior, N. (1985), "Numerical calculations of laminar and turbulent natural convection in water in rectangular channels heated and cooled isothermally on the opposing vertical walls", *Int J. Heat Mass Transfer*, Vol. 28, pp. 125-38.

Patankar, S.V. (1980), *Numerical Heat Transfer and Fluid Flow*, McGraw-Hill, New York, NY.

Powe, R.E., Carley, C.T. and Bishop, E.H. (1969), "Free convection flow pattern in cylindrical annuli", *ASME J. Heat Transfer*, Vol. 91, pp. 310-14.

Saitoh, T. and Hirose, K. (1989), "High accuracy benchmark solutions to natural convection in a square cavity", *Comput. Mech.*, Vol. 4, pp. 417-27.

Tao, W.Q. (2001), *Numerical Heat Transfer*, 2nd ed., Xi'an Jiaotong University Press, Xi'an.

Thummes, G., Schreiber, M., Landgraf, R. and Heiden, C. (1997), "Convective heat losses in pulse tube coolers: effect of pulse tube inclination", *Cryocoolers*, Vol. 9, pp. 393-402.

Wei, J.G. and Tao, W.Q. (1996a), "Numerical study of natural convection in a vertical annulus with constant heat flux on the inner wall", *Int. J. Numer. Methods Heat Fluid Flow*, Vol. 6, pp. 31-46.

Wei, J.G. and Tao, W.Q. (1996b), "Three-dimensional numerical simulation of natural convection heat transfer in an inclined cylindrical annulus", *J. Thermal Sci.*, Vol. 5, pp. 175-83.